Journal of
www. biophotonics-journal.org
BIOPHOTONICS

WILEY-VCH

J. Biophotonics **5**, No. 2, 185–193 (2012) / **DOI** 10.1002/jbio.201100050

Journal of BIOPHOTONICS

FULL ARTICLE

Laser tissue welding analyzed using fluorescence, Stokes shift spectroscopy, and Huang-Rhys parameter

*Vidyasagar Sriramoju and Robert R. Alfano**

Institute for Ultrafast Spectroscopy and Lasers, Department of Physics, The City College of New York, 160 Convent Avenue, New York, NY 10031, USA

Received 12 June 2011, revised 27 September 2011, accepted 28 September 2011
Published online 14 November 2011

Key words: laser tissue welding, Huang-Rhys factor, Stokes shift, resonance energy transfer, Raman spectroscopy, fluorescence, water and collagen in tissue

Near infrared (NIR) continuous wave laser radiation at the 1,450 nm wavelength was used to weld porcine aorta and skin samples via the absorption of combitional vibrational modes of native water in the tissues. The fluorescence spectra were measured from the key native molecules of welded and non-welded tissues at specific excitation and emission wavelengths from collagen, elastin, and tryptophan. The changes in the fluorescence intensities and differences in Stokes shift ($\Delta\nu_{ss}$) of key native fluorophores were measured to differentiate the Huang-Rhys parameter values (S) of the chromophores. The strength of coupling depends on the local electron-vibration intra-tissue molecular environment and the amount of polar solvent water surrounding the net charges on collagen, elastin, and tryptophan. The S values for both non-welded and welded tissues were almost the same and less than 3, suggesting minimal changes in the local molecular environment as a result of welding.

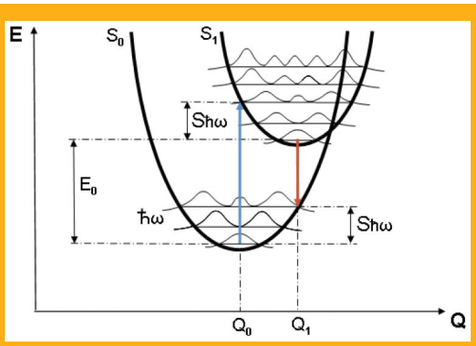

Energy configuration coordinate diagram and transitions of an organic molecule depicting the effects of tissue polar solvents and net changes surrounding native fluorophores on their Stokes shifts and Franck-Condon energy states.

1. Introduction

Laser tissue welding (LTW) is a procedure for fusing or uniting edges of two opposing animal or human tissue segments by the laser photoexcitation of their native chromophores and water, only light acts as the bonding catalyst. The fusion of the incised tissues as a result of near-infrared (NIR) laser interaction was found to be almost as effective as conventional sutures with silk. Heat generated from the laser energy absorption by combination vibrational modes of water causes, either directly or indirectly, the formation of cross-links between proteins in the tissues on either side of the weld line. No extrinsic agents (dyes or solder) were used in this study of bonding in LTW. This vibration excitation method for bonding the tissues can be used for those structures that are difficult to suture; examples include blood vessels, gallbladder, visceral structures, nerves, and arterial anastomoses. LTW can also be used in endoscopic surgery.

* Corresponding author: e-mail: ralfano@sci.ccny.cuny.edu

Journal of
BIOPHOTONICS

Over the past few years, LTW technology has been successfully shown to reduce the risk of foreign body reaction; to minimize the chances of serious infections, local immune reactions, or toxicity; to reduce surgical time; to improve wound healing; to reduce the amount of scar tissue formation; to shorten operating time; and to be ideally suited for applications in which suturing and stapling are difficult [1–3].

The welding of the tissue occurs by the fusion of collagen fibers [2–4]. Collagen is the main structural protein of the body. Collagen molecules, after secretion by the cells, accumulate into characteristics fibers responsible for the functional integrity of such tissues as cornea, bone, skin, cartilage, and tendon. Collagen contributes to the structural framework of other tissues, such as blood vessels and most organs. Cross-links between adjacent molecules are a prerequisite for the collagen fibers to survive the physical stresses to which they are exposed. Collagen forms a triple helical structure, and the most common triplet combination in collagen is Gly-Pro-Hyp [5–9]. NIR LTW involves the partial denaturation and renaturation of collagen that results from the laser-tissue interaction. Collagen is measured using fluorescence.

The molecular mechanisms underlying LTW due to optical excitation are depicted in Figure 1. Alfano's group used the NIR absorption band of water at 1,450 nm for the energy transfer to the structural proteins of cell membranes for the molecular relinking of cut tissues [10, 11]. During welding, water in the tissue absorbs the NIR laser energy by vibrational overtones and combinations of water modes (υ_1, υ_2, υ_3) and subsequently heats the collagen molecules via energy transfer as the temperature rises to 60 °C. NIR laser energy at 1,450 nm excites the combination vibrational mode ('1, 0, 1') of water [12, 13], thereby disrupting the H-bonding in collagen molecules, resulting partial reversible denaturation. The reformation of covalent and/or noncovalent bonding of the tissue protein molecules takes place as the tissue cools [8, 9].

Fluorescence spectroscopy is a noninvasive method used to measure electronic and vibrational transitions of various photoexcited chromophores in complex host tissue structures [14]. In tissue, several natural fluorophores are: collagen, elastin, and tryptophan, which can be photoexcited by ultraviolet light. In the ultraviolet and visible regions of the spectrum, the fluorescence can be detected. Native fluorescence imaging identifies molecules in tissue samples from the use of different emission and excitation wavelengths. The shifts of absorption and emission of fluorophores in host determines the strength of interaction between electrons of fluorophores and surrounding host molecules. The Huang-Rhys parameter S determine the strength of interaction and quantifies lattice relaxation of electronic states of photoexcited molecule.

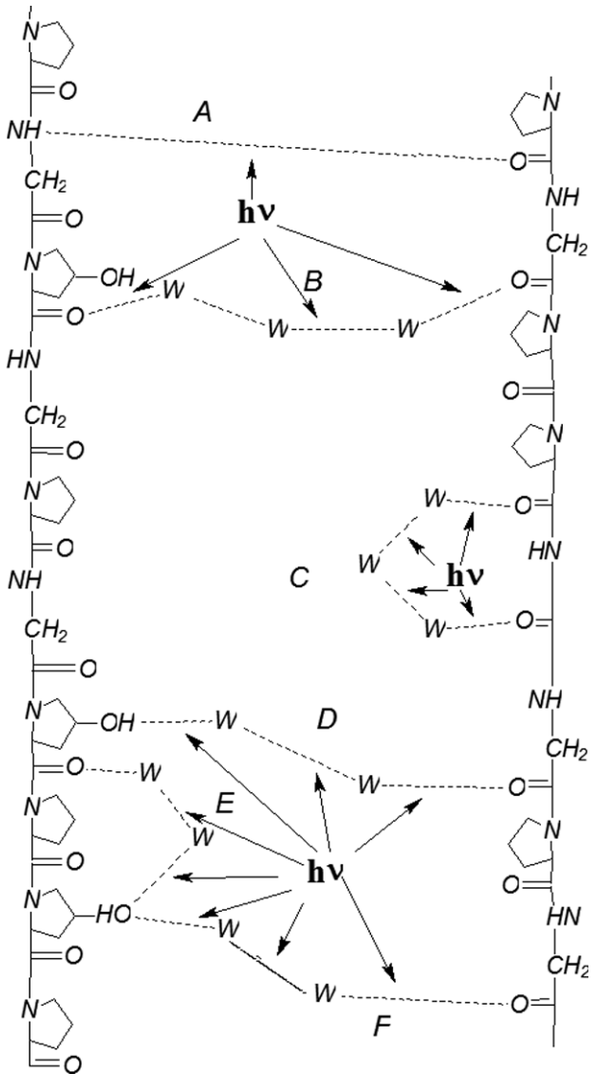

Figure 1 A schematic depiction of the Molecular mechanisms of laser tissue welding –: The arrows show the sites of interchain and intrachain H-bonds that are reversibly dissociated as a result of energy transfer from water molecules excited by "$h\nu$" of NIR laser radiation.

In this paper, the fluorescence spectroscopy was used before and after LTW to measure and analyze the effects of LTW on biochemical composition of tissues and changes in collagen, tryptophan, and elastin. The strength of electronic-vibration states in the tissue were measured by Huang-Rhys (S) parameters for welded and unwelded tissues. The peak excitation and emission wavelengths of these key fluorophores collagen, elastin, tryptophan in native tissues and laser-welded tissues were identified by fluorescence spectroscopy. Stokes shifts and Huang-Rhys parameters (S) were measured to determine the minimal effects of LTW on molecular scale.

The fluorescence spectra were acquired from welded porcine aortas and skin at three pairs of excitation and emission wavelengths. These wavelengths corresponded to the excitation and emission bands of collagen, elastin, and tryptophan. The changes in fluorescent intensity and Stokes shifts of these three molecules in normal and laser-welded tissues were studied in order to evaluate the extent of denaturation of proteins as a result of LTW. The electronic transitions take place more rapidly than the nucleus motion since electrons are lighter than nuclei. The Born-Oppenheimer principle separates the electron from vibration wave function. The spectral shifts in absorption and emission are due to overlap of initial and final vibrational wave functions in the transition. The strength of electron and vibration interaction is proportional to Huang-Rhys parameter S, which shifts the energy state location in configuration coordinates Q due to local surrounding host dipoles [15]. The Franck-Condon states are related to the excited state molecule characterized by the altered spatial distribution of the electrons that is not the minimum energy configuration of the excited state as a result of absorption of a photon [16, 17]. Here, only electron distribution is affected, not the positions of nuclei or bond lengths and angles, because the absorption timescale is approximately one femtosecond; hence, there is no net change in the molecular geometry (see Figure 2). Upon activation in the excited state, readjustment of the molecular structure occurs. The optical properties of the native tissue chromophores are affected by solvation, due to the polar nature of water and the charges on the molecules in tissues that alter the molecular geometry. Therefore, the Franck-Condon energies are affected.

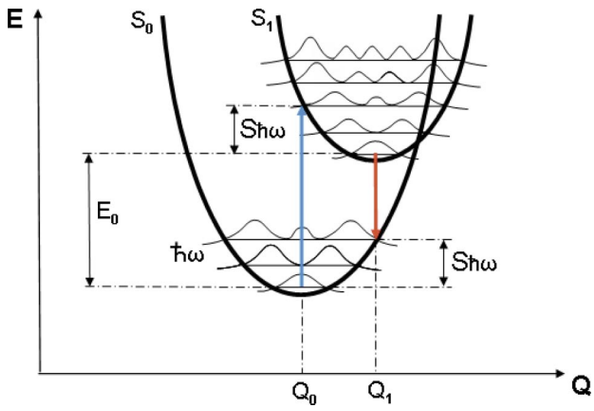

Figure 2 (online color at: www.biophotonics-journal.org) Energy configuration coordinate diagram and transitions of an organic molecule depicting the effects of tissue polar solvents and net changes surrounding native fluorophores on their Stokes shifts and Franck-Condon energy states. The downward-curved dotted arrows denote vibrational relaxation states which vary with surrounding solvent properties. The Huang-Rhys factor (S) is the measure of the strength of coupling between shift of the ground and excited states in the fluorophore's manifold.

The electronic and vibrational states of the organic molecules are best represented in electron ground states (S_0) and excited states (S_1) in energy versus configuration coordinate space Q as shown in Figure 2 [18–21]. The Stokes shift is the difference between the absorption peak and the emission peak. The differences in Stokes values are due to differences in excitation energies of electrons, due to electron-solvent interaction. The Huang-Rhys parameter (S) is the measure of the strength of the level of interaction between excited and ground states of electrons. The electron states of the molecule center in host are coupled to the vibrations by electron-vibration interaction [21]. The motion of electron and vibration in ground state and excited state are represented by E–Q diagram shown in Figure 2. The S value can be obtained by measuring the Stokes shift of the chromophore from the excitation and emission maxima. The Stokes shift is:

$$E_{\text{Stokes}} = h\,\Delta\nu_{\text{Stokes}} = (h\nu_{\text{Absorption}}) - (h\nu_{\text{Emission}}) \quad (1)$$

and

$$h\,\Delta\nu_{\text{Stokes}} = 2Sh\nu_q \quad (2)$$

where "S" is the Huang-Rhys factor and "ν_q" is the average vibrational frequency. The displacement of the excited state from the ground state minima 'Q_0" that depends on "S" value and is given by:

$$Q_0 = \sqrt{\frac{Sh}{\nu_q}} \quad (3)$$

The formation of luminescence bands from ions, atoms, and molecules inside the host are represented by transitions of electrons and vibrations in Figure 2. The resonance energy transfer from excited electrons between molecules of collagen and water with collagen is of the Förster type; it is related to S by activation energy $E_a = E_S/4$ and Förster distance $R_0 \leq 8$ nm [16–21]. The dynamics of vibrational energy transfer from photoexcited ions to host vibrations is described experiments by Demos [22] and Calistru [23]. The distance between collagen and water with collagen was less than or equal to 10 nm. For LTW, the NIR absorption by water involves combinations and overtones (ν_1, ν_2, ν_3) of symmetric stretch ν_1 at 3280 cm^{-1}, asymmetric stretch ν_3 at 3491 cm^{-1} and bending mode ν_2 at 1624 cm^{-1}. At 1472 nm, the absorption is due to vibrations of (1, 0, 1) [12, 13].

Journal of
BIOPHOTONICS

2. Methods and materials

2.1 Sample preparation

The animal experiments done in this study were approved by the IACUC of the City College of New York. The porcine aorta and skin samples used for the LTW were purchased from a USDA-approved animal slaughterhouse (Countryside Quality Meats, Inc., Union City, MI). The porcine tissues were shipped on wet ice to our laboratory. The received samples were washed with 0.9 percent saline solution. The aortas were opened by incision along their long axes; the skin was shaved. The samples were cut into rectangular pieces of 20×100 mm, prepared with the long axis of the rectangle parallel to the long axis of the entire tissue. Then, these pieces were sectioned parallel to the circumference of the aorta into specimens measuring 20×10 mm. Each specimen was bisected into 10×10 mm pieces, which were then welded using an eight-line pattern. The beam was focused on the half thickness (≈ 1 mm) of the tissue.

2.2 Laser system

Figure 3 is a schematic representation of the laser welding system used in this study. The erbium fiber laser used was a B & W Tek model BWF2 (B & W Tek, Inc., Newark, DE) that emits at a wavelength of 1,455 nm and has a maximum power level of 2 W. The emission wavelength of the erbium fiber laser in the NIR range corresponds to one of the absorption bands of water. The water absorption band peak occurs at 1,450 nm from the combination of vibrations of (1, 0, 1). This absorption band covers a range from 1,380 to 1,600 nm. For the erbium fiber laser, a red LED, included as a component in the B&W Tek laser, was coupled into the fiber and used to align the NIR welding light.

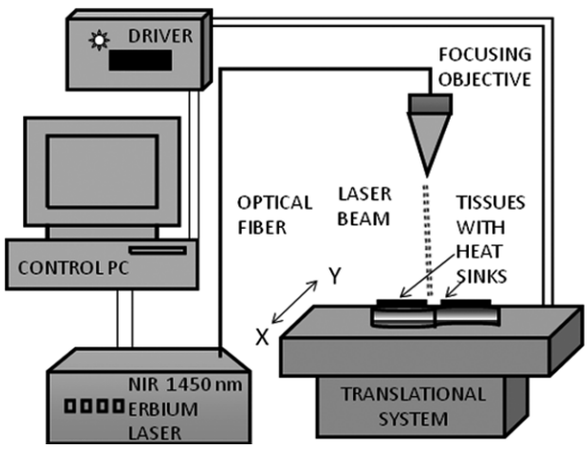

Figure 3 The schematic diagram of LTW setup.

The porcine aorta samples were placed on glass microscope slides and fixed on the translational stage of a motion control system manufactured by Aerotech, Inc. (Pittsburgh, PA), which comprised the following components: a Unidex 500 PCI-based controller, a DR500 motor driver and chassis, an ATS100-050 linear stepping motor, an ATS50-50 linear stepping motor, test software and a software development kit, cables, and brackets. The function of the motion control system was to physically move the tissue under the laser beam in a pattern directed by the movement software. A Thorlabs MeterMate power meter (Thorlabs, Newton, NJ) was used to measure the laser power at the end of the objective lens prior to performing each of the tissue welds.

2.3 Tissue welding parameters

All of the porcine tissue samples were welded with NIR laser radiation at the 1,450 nm wavelength and with 300 mW–900 mW of power. The total number of patterns per weld was 56, and each pattern had eight lines. In each pattern, four lines were focused directly on the weld line, two lines were at +/−35 μm and another two lines were at +/−70 μm from the weld line, thus covering a total of 140 μm across.

2.4 Raman spectroscopy

The average phonon frequency, ν_q, was obtained by measuring the Raman spectra to determine ν_i from collagen, elastin, and tryptophan chemicals. The weighted average phonon value is calculated by using the following formula:

$$\nu_q = \frac{\sum a_i \nu_i}{\sum_{i=1} a_i} \tag{4}$$

where "a_i" is the height of the Raman peak at ν_i

2.5 Fluorescence spectroscopy

The fluorescence spectra of welded and non-welded porcine aortas and skin tissues were measured with an LS 50B fluorescence spectrometer (Perkin-Elmer Corporation, Shelton, CT). Three pairs of fluorescence emission and excitation spectra (Table 1) were obtained from the external and internal surfaces of

Table 1 Parameters of excitation and emission ranges of the key fluorophores in the tissues.

Fluorophore	Excitation spectra range in nm	Emission spectrum range in nm
Collagen	280–360	360–400
Tryptophan	230–300	320–380
Elastin	300–400	380–450

the welded and non-welded porcine aortas and skin tissues. The LS 50B has a broadband-pulsed xenon flash lamp for excitation and dual monochromators for independent control of excitation and emission wavelengths. It also has a gated photomultiplier tube to detect the emitted signals. All emission and excitation spectra presented in this paper were obtained with identical instrument parameters (slit widths of 2.5 nm for both emission and excitation spectra, integration times, optical filters, a scanning speed of 120 nm/minute, etc.). The fluorescence data was acquired as ASCII files by the PC attached to the LS 50B. These data files were plotted and analyzed using Origin 7.0 software (Originlab Corp., Northampton, MA). The tissue samples were pumped with 280 nm wavelength while measuring emissions covering from 300 to 500 nm. The tissue depths pumped is $\leq$0.5 mm. The peaks found at 340, 380, and 410 nm belonged to tryptophan, collagen, and elastin, respectively.

3. Results

The fluorescence spectra from welded and non-welded porcine aorta and skin specimens are shown in Figures 4 and 5. The tissues, excited with a

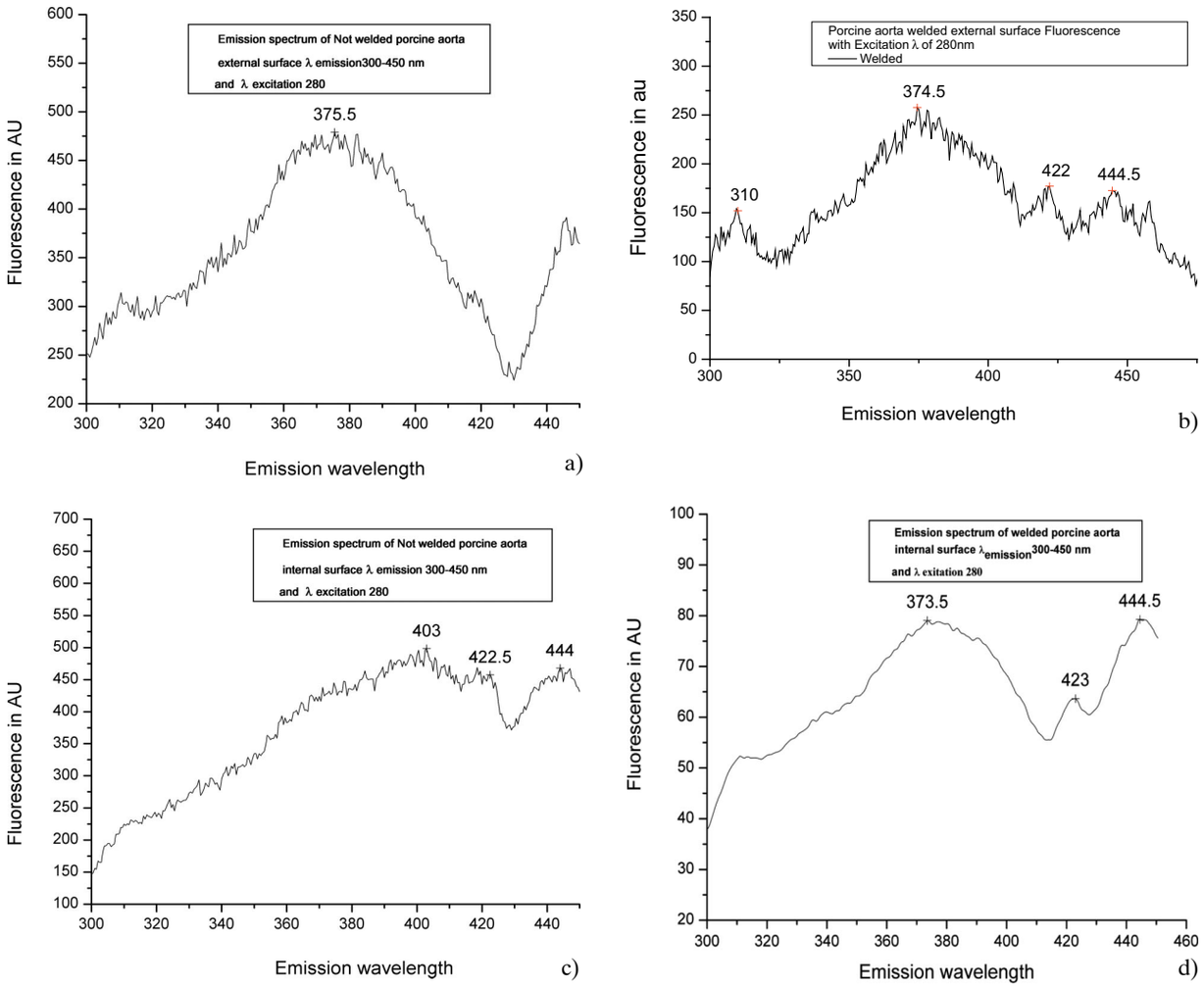

Figure 4 The fluorescence spectra external and internal surfaces of non-welded (**a** and **c**) and welded (**b** and **d**) porcine aorta tissues excited at 280 nm.

Journal of
BIOPHOTONICS

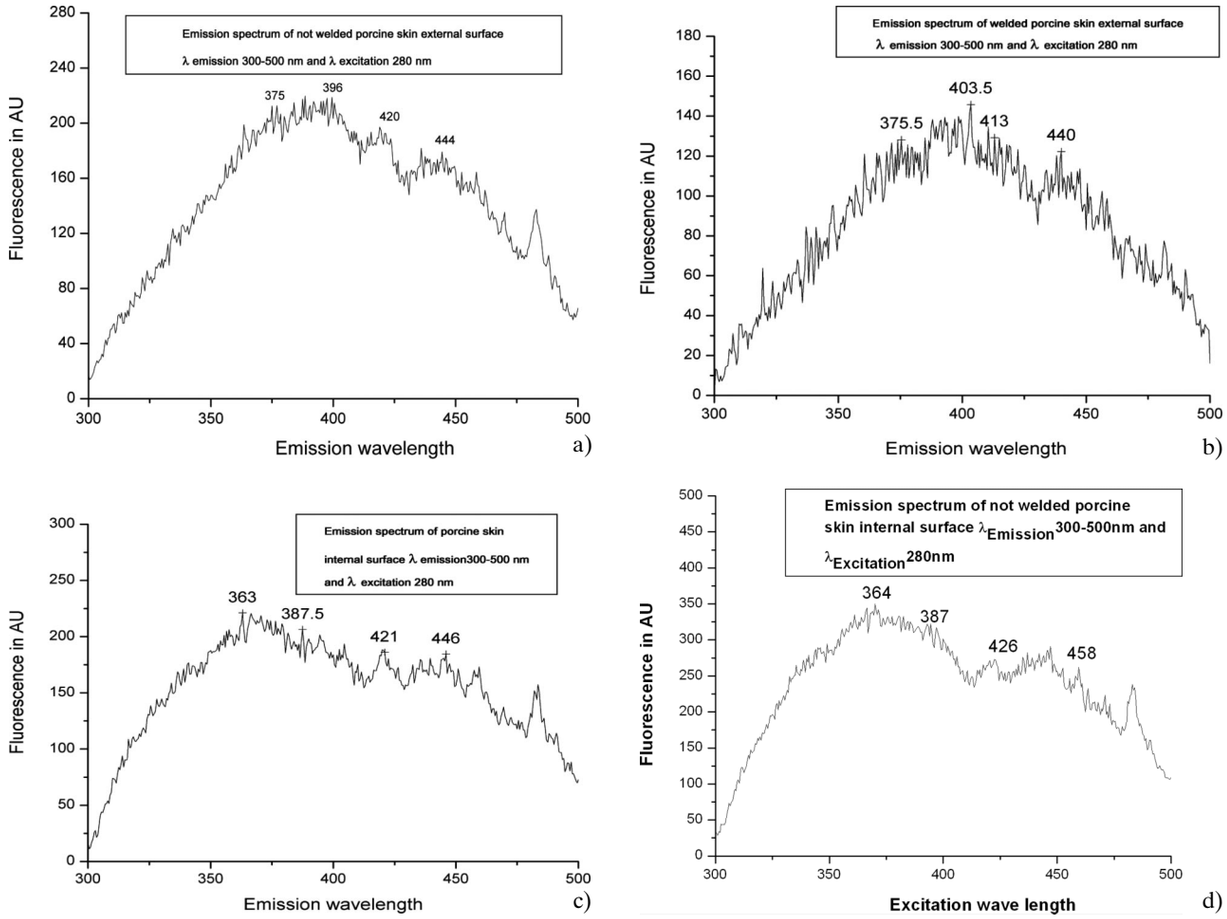

Figure 5 The fluorescence spectra external and internal surfaces of non-welded (**a** and **c**) and welded (**b** and **d**) porcine skin tissues excited at 280 nm.

Table 2 Fluorescence Stokes changes in external side of porcine aorta.

	Tissue sample and Fluorophore	Peak Excitation (nm)	Peak Emission (nm)	Stokes Shift (nm)	Huang Rhys factor
Porcine aorta	Collagen welded ext side	335.0	396.0	61.0	1.96
Porcine aorta	Collagen non-welded ext side	345.0	372.0	28.0	0.90
Porcine aorta	Elastin ext welded side	340.0	422.0	82.0	2.34
Porcine aorta	Elastin non-welded ext side	343.0	413.0	70.0	2.02
Porcine aorta	Tryptophan ext welded side	270.0	367.0	97.0	2.88
Porcine aorta	Tryptophan non-welded ext side	270.0	376.0	106.0	3.07

Table 3 Fluorescence Stokes changes in internal side of porcine aorta.

Tissue sample	Fluorophore	Peak Excitation (nm)	Peak Emission (nm)	Stokes Shift (nm)	Huang Rhys factor
Porcine aorta	Collagen welded int side	333.0	379.0	46.0	1.55
Porcine aorta	Collagen non-welded Int side	343.0	401.0	58.0	1.79
Porcine aorta	Elastin welded int side	345.0	408.0	63.0	1.83
Porcine aorta	Elastin non-welded Int side	349.0	421.0	72.0	2.00
Porcine aorta	Tryptophan welded int side	270.0	373.0	103.0	3.00
Porcine aorta	Tryptophan non-welded Int side	280.0	376.0	96.0	2.68

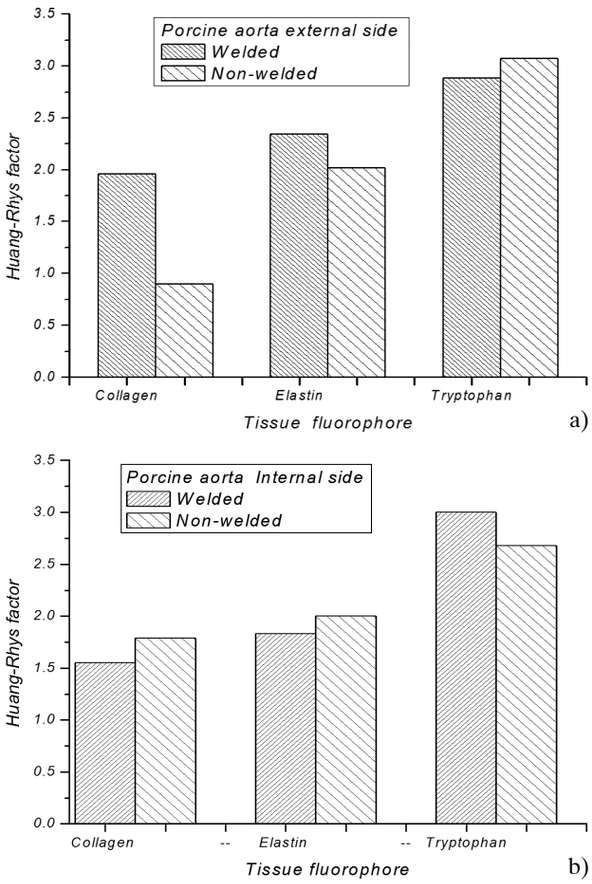

Figure 6 (**a**, **b**): Huang-Rhys factor in differences between welded and non-welded porcine aorta external and internal surfaces.

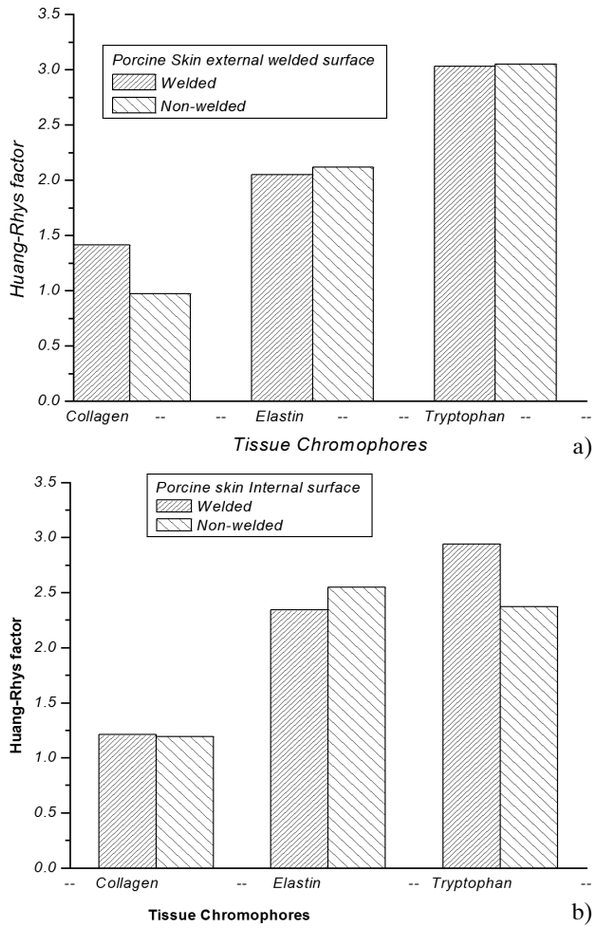

Figure 7 (**a**, **b**): Huang-Rhys factor in differences between welded and non-welded porcine skin external and internal surfaces.

280 nm wavelength, revealed a broad band of emissions with peaks corresponding to the emission bands of collagen, elastin, and tryptophan. The fluorescence spectroscopic curves were acquired from both outer and inner surfaces at the weld line of all tissue specimens. Both the aortas and skin specimens were observed to exhibit buckling on their outer surfaces facing the welding laser; the skin suffered more severe buckling than the aortas. This phenomenon in skin may have been because skin has large quantities collagen; aortic tissue has an abundance of elastin, which has greater heat resistance than collagen. Examination of the fluorescence spectra of the aortas revealed a higher degree of uniformity than skin.

Table 4 Fluorescence Stokes changes in external side of porcine skin.

Tissue sample	Fluorophore	Peak Excitation (nm)	Peak Emission (nm)	Stokes Shift (nm)	Huang Rhys factor
Porcine skin	Collagen welded Ext side	350.0	396.0	46.0	1.41
Porcine skin	Collagen non-welded Ext side	348.0	378.0	30.0	0.97
Porcine skin	Elastin welded Ext side	345.0	417.0	72.0	2.05
Porcine skin	Elastin non-welded Ext side	345.0	420.0	75.0	2.12
Porcine skin	Tryptophan welded Ext side	271.0	376.0	105.0	3.03
Porcine skin	Tryptophan non-welded Ext side	270.0	375.0	105.0	3.05

Journal of
BIOPHOTONICS

Table 5 Fluorescence Stokes changes in internal side of porcine skin.

Tissue sample	Fluorophore	Peak Excitation (nm)	Peak Emission (nm)	Stokes Shift (nm)	Huang Rhys factor
Porcine skin	Collagen welded int side	338.0	374.0	36.0	1.21
Porcine skin	Collagen non-welded int side	337.0	372.0	35.0	1.19
Porcine skin	Elastin welded int side	340.0	422.0	82.0	2.34
Porcine skin	Elastin non-welded int side	334.0	422.0	88.0	2.55
Porcine skin	Tryptophan welded int side	270.0	370.0	100.0	2.94
Porcine skin	Tryptophan non-welded int side	270.0	345.0	75.0	2.37

4. Discussion

The Stokes shift values were obtained from the absorption and emission maxima from the fluorescence spectra shown in Figures 4 and 5. The Huang-Rhys parameter (S) values were calculated and displayed in Figures 6 and 7. Tables 2 to 5 show the fluorescence and absorption peaks, Stokes shifts, and S values from the various tissue samples. The Stokes shift changes in welded and non-welded porcine aortas. The $S \leq 3$ shows weak coupling. In addition, after welding, the collagen, elastin, and tryptophan intensities also decreased. The spectra from porcine skin showed that the external surface was less uniform than the internal surface. This effect could be due to the roughness and presence of residual hairs on the external surface of the skin. For both external and internal surfaces, no major differences were found in Stokes shift between the welded and non-welded skin. The dips in fluorescence spectra is attributed to self absorption due to presence of hemoglobin in the tissue [24]. The most intense transition of hemoglobin's absorption in uv/blue fluorescence is at about 430 nm corresponding to the Soret band. The dip is shown in some of the data (see Figures 4 a–d). The fluorescence intensities of collagen, elastin, and tryptophan decreased in the welded samples. This may have resulted from a loss of water and changes in the scattering of light. The previous results by our group (10) with 1450 nm CW, NIR laser on "*ex vivo*" porcine aorta and skin with similar welding parameters achieved successful welds with good tensile strengths. Moreover, 1500 nm wavelength fs pulse LTW gave better results for in vivo experiment [25]. In those studies histopathological evaluations laser welded tissues using optical and scanning electron microscopy revealed no significant thermal injury of tissues, no changes in cellular morphology and no structure and orientation of collagen fibers. It is concluded that the laser powers used will not cause the total denaturation of the proteins. In any such event of total protein denaturation due to laser, will not result in the tissue fusion.

6. Conclusion

Using the native fluorescence of tissue allows the evaluation of local changes in collagen, elastin, and tryptophan. Fluorescence spectroscopy can be used to develop a noninvasive diagnostic tool for *in vivo* evaluation of weld quality and collagen during LTW and also to understand fundamental molecular mechanisms. The small changes in S values (less than or almost equal to 3) for both welded and non-welded tissues from this study indicate that collagen, elastin, and tryptophan undergo subtle changes on the molecular scale as a result of laser photoexcitation during LTW. Native fluorescence demonstrates the molecular changes in tissues after the heat treatment. Raman scattering showed similar results [25] of minimal effects for LTW using fs pulses at 1500 nm. With this approach, it is possible to evaluate *in vivo* laser treatments for laser photocoagulation, interstitial hypothermia, welding, collagen growth and plastic surgery.

Acknowledgements This work was supported by NIH RO1 EB000297-6. We thank Ms Liu, Ms Rakhi Podder, Mr. Rahul Chakraverty, Mr. Ronex Muthukattil worked on the project at various stages.

Vidyasagar Sriramoju is a physician pathologist. He graduated with medical degree in 1991 from Osmania Medical College, Osmania University, Hyderabad, India. He moved to United States in 1998 to pursue a career in biomedical research working at Pennsylvania State University. In 2002, he started working at City College of New York as a postdoctoral researcher in neurobiology. In 2004 he moved to the Institute for Ultrafast Spectroscopy and Lasers at City College of New York to pursue interdisciplinary research in biomedical photonics with focus on laser tissue welding, tissue imaging, molecular diagnostics, and biological spectroscopy. In 2010 Dr. Sriramoju started working for Industry in the areas of molecular diagnostics and biophotonics.

Robert R. Alfano, Distinguished Professor of Science and Engineering at The City College of the City University of New York, is a pioneer in the application of light and photonics technology to the study of biomedical systems and a leader in inventing novel light sources and developing ultrafast laser spectroscopic techniques. His research achievements include pioneering contributions in developing laser spectroscopic and optical biomedical imaging techniques for noninvasive, pain-free detection and diagnosis of diseases. He has received his Ph.D. in physics from New York University. In 2008, he received the OSA Charles Hard Townes Award for supercontinuum discovery and tunable laser development.

References

[1] M. C. Oz, M. R. Williams, J. E. Souza, H. Dardik, M. R. Treat, L. S. Bass, and R. Nowygrod, J. Clin. Laser Med. Surg. **11**(3), 123–126 (1993).
[2] R. Schober, F. Ulrich, T. Sander, H. Dürselen, and S. Hessel, Science **232**(4756), 1421–1422 (1986).
[3] L. S. Bass, M. R. Treat, C. Dzakonski, and S. L. Trokel, Microsurg. **10**(3), 189–193 (1989).
[4] L. S. Bass, N. Moazami, J. Pocsidio, M. C. Oz, P. LoGerfo, and M. R. Treat, Laser Surg. Med. **12**(5), 500–505 (1992).
[5] B. Brodsky and A. V. Persikov, Ad. Protein Chem. **70**, 301–339 (2005).
[6] A. V. Persikov, J. A. Ramshaw, and B. Brodsky, J. Biol. Chem. **280**(19), 19343–19349 (2005).
[7] A. V. Persikov, J. A. Ramshaw, A. Kirkpatrick, and B. Brodsky, Biochemistry-US 39(48), 14960–14967 (2000).
[8] B. Brodsky and J. A. Ramshaw, Matrix Biol. **15**(8–9), 545–554 (1997).
[9] J. Bella, B. Brodsky, and H. M. Berman, Structure **3**(9), 893–906 (1995).
[10] T. K. Gayen, A. Katz, H. E. Savage, S. A. McCormick, M. Al-Rubaiee, Y. Budansky, J. Lee and R. R. Alfano, J. Clin. Laser Med. Surg. **21**(5), 259–269 (2003).
[11] H. E. Savage, R. K. Halder, U. Kartazayeu, R. B. Rosen, T. Gayen, S. A. McCormick, N. S. Patel, A. Katz, H. D. Perry, M. Paul, and R. R. Alfano, Laser Surg. Med. **35**(4), 293–303 (2004).
[12] R. Lemus, J. Mol. Spectrosc. A **225**, 73–92 (2004).
[13] S. Yu. Venyaminov and F. G. Prendergast, Anal. Biochem. **248**, 234–245 (1997).
[14] J. Tang, F. Zeng, J. M. Evans, B. Xu, H. Savage, P. P. Ho, and R. R. Alfano. J. Clin. Laser Med. Surg. **18**(3), 117–123 (2000).
[15] K. Huang and A. Rhys, Proc. Roy. Soc. A **204**, 406 (1950).
[16] A. S. Coolidge, H. M. James, and R. D. Present, J. Chem. Phys. **4**, 193–211 (1936).
[17] R. R. Alfano and Y. Yang, IEEE J. Sel. Top. Quant. Electron. **9**, 148 (2003).
[18] S. H. Lin and W. Z. X. Lin, Phys. Rev. E **47**, 3698–3706 (1993).
[19] T. Markvart and R. Greef, J. Chem. Phys. **121**(13), 6401–6405 (2004).
[20] M. Fox, Optical properties of solids (Oxford Press, Oxford, 2008), chap. 9.
[21] B. K. Ridley, Quantum processes in semiconductors (Oxford Press, Oxford, 1982), chap. 2.
[22] S. G. Demos, D. M. Calistru, and R. R. Alfano, Phys. Lett. **68**, 1195–1197 (1996).
[23] D. M. Calistru, S. G. Demos, and R. R. Alfano, Phys. Rev. Lett. **78**, 374–377 (1997).
[24] C. H. Liu, G. C. Tang, A. Pradhan, W. L. Sha, and R. R. Alfano, Las. Life Sci., **3**, 167 (1990).
[25] A. Alimova, R. Chakraverty, R. Muthukattil, S. Elder, A. Katz, V. Sriramoju, S. Lipper, and R. R. Alfano, J. Photochem. Photobiol. B **96**, 178–183 (2009).